Quantum Monte Carlo study of the two-dimensional ferromagnet

G. J. Conduit

Cavendish Laboratory, J.J. Thomson Avenue, Cambridge CB3 0HE, United Kingdom

We present quantum Monte Carlo calculations that probe the paramagnet-ferromagnet phase transition in a two-dimensional Stoner Hamiltonian. With a screened Coulomb interaction we observe a first-order ferromagnetic transition for short screening lengths, and a second-order transition with a longer screening length, accompanied by a rising critical interaction strength. Finally, we discuss the consequences of our results for an ultracold atomic gas with finite ranged interactions.

I. INTRODUCTION

Layered systems that display magnetic correlations have emerged as an important test bed of strongly correlated physics. The Stoner Hamiltonian represents the simplest possible metallic system that undergoes a ferromagnetic transition. Since a mean-field analysis[1] predicts a second-order transition, in the vicinity of the low temperature transition Hertz[2] predicted that quantum fluctuations would drive critical behavior. However, it has recently been predicted that quantum fluctuations are even stronger than envisaged by Hertz and drive phase reconstruction through a first-order ferromagnetic transition,[1,3–7] consistent with the phase transition observed in the quasi-two-dimensional systems $Sr_{3-x}Ca_xRu_2O_7$,[8,9] Sr_2RuO_4,[10] $La_xSr_{2-x}RuO_4$,[11] Ca_2RuO_4,[12] and UGe_2.[13–15] The importance of the quantum fluctuations in driving this phase reconstruction motivates a careful theoretical analysis of the Stoner Hamiltonian. However, analytical studies[1,3–7] of the magnetic transition rely on a perturbation theory in the interaction strength, whereas in reality the interactions are strong and the quantum fluctuations dominant. To probe the phase transition in the nonperturbative regime we perform and present the first quantum Monte Carlo (QMC) calculations of the two-dimensional itinerant ferromagnet with short-ranged interactions. We complement this with the first analytical study of the ferromagnetic transition in two dimensions with a screened Coulomb interaction that allows us to be the first to calculate the dependence of the tricritical point temperature on screening length. The QMC calculations employ a fixed node approximation, tempered by backflow corrections, so should complement and improve upon the accuracy of the analytical findings.

An ultracold atomic gas could be an attractive alternative realization of the Stoner Hamiltonian. Recent experiments on the three-dimensional system,[16] and polaron systems[17,18] have delivered some evidence for ferromagnetic ordering,[19–21] though a competing loss process provides an alternative explanation.[22,23] Accurate QMC calculations that pin the transition down should help guide future experiments that could realize a Hamiltonian analogous to the Stoner system.[1,7,24–26] The theoretical and experimental study of the idealized two-dimensional ultracold atomic gas also presents an opportunity to shed light on high temperature superconductivity where antiferromagnetism competes with the d-wave superconducting phase.[1]

In this paper we present QMC calculations to analyze the paramagnet-ferromagnet transition in two dimensions. To connect to the solid state the QMC calculations are performed first with the screened Coulomb interparticle potential and later the results are compared to the square well potential. Both interparticle potentials are characterized by a range parameter that we vary to gauge the consequences of screening in the solid state, and the interaction effective range in the cold atom gas. Combining our QMC results with a complementary analytical order-by-disorder approach allows us to derive the phase diagrams shown in Fig. 1 at finite temperatures. The phase diagram shows that the paramagnet-ferromagnet transition reverts from first to second order on increasing the screening length, and the corresponding critical interaction strength increases. The introduction of a finite interaction range with $k_F b > 0$ increases the critical interaction strength, and lowers the tricritical point temperature to be in line with experimental values. Finally, we adapt our formalism to assess the opportunity to observe ferromagnetic correlations in an ultracold atomic gas.

II. FORMALISM

To model the ferromagnet we focus on the modified Stoner Hamiltonian,

$$\hat{H} = \sum_{\mathbf{p},\sigma} \epsilon_{\mathbf{p}} \hat{n}_{\mathbf{p}\sigma} + \int\int d\mathbf{r}_\uparrow d\mathbf{r}_\downarrow g(\mathbf{r}_\uparrow - \mathbf{r}_\downarrow)\hat{n}_{\mathbf{r}_\uparrow\uparrow}\hat{n}_{\mathbf{r}_\downarrow\downarrow}, \quad (1)$$

where $\epsilon_{\mathbf{p}} = p^2/2$ is the dispersion, $n_{\mathbf{p}\sigma}$ is the fermion occupancy in momentum space, $n_{\mathbf{r}\sigma}$ in real space, spin $\sigma \in \{\uparrow,\downarrow\}$, and we adopt atomic units with $\hbar = m = 1$ throughout. To simulate the interparticle repulsion we use a screened Coulomb interaction parametrized as $g(r) = g e^{-r/b}/2\pi br$ acting between opposite spin particles separated by a distance r. It is characterized by a screening radius b and interaction strength g. To validate our results we also study the square potential of radius R, $g(r) = g\theta(R - r)/\pi R^2$ with Heaviside function θ, whose interaction strength and screening parameter are related to the screened Coulomb interaction through a momentum-space expansion.[27] The interparticle potentials are defined so that they have the simple momentum space forms $g_{\mathbf{q}} = g/\sqrt{1 + b^2 q^2}$ and $g(1 - R^2 q^2/8)$, respectively. This allows them to be used within our analytical formalism. These definitions mean that the ferromagnetic transition in the mean-field approximation emerges at the critical interaction strength $g_{MF} = 2\pi$. To evaluate the energy of the electrons we employ two complementary techniques, a quantum Monte
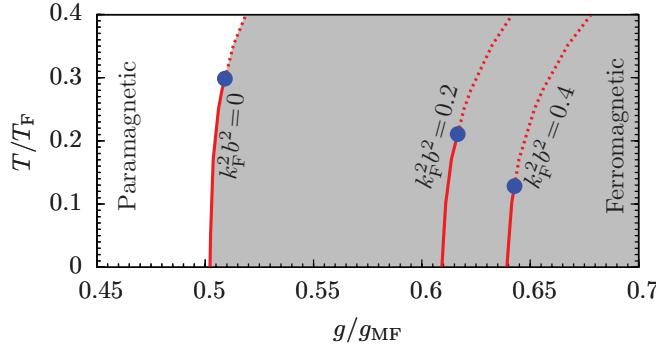
FIG. 1. (Color online) The phase diagram for the system from the paramagnetic to ferromagnetic phase (shaded gray). The red solid line shows the first-order ferromagnetic transition and the dashed line the second-order transition with the tricritical point highlighted by the blue dot. The three lines denote boundaries with a screening length of $k_F^2 b^2 = 0$, $k_F^2 b^2 = 0.2$, and $k_F^2 b^2 = 0.4$.

Carlo calculation limited only by a fixed node approximation, and an analytical evaluation of the free energy derived by a functional integral formalism. The mechanics of both methods are outlined below before we study the resulting phase diagrams.

A. Quantum Monte Carlo formalism

To seek and calculate the ground state of the Hamiltonian we perform QMC simulations with the code CASINO.[28] This method optimizes a trial wave function at zero temperature, and finds the exact ground state subject to the nodal surface of the wave function being fixed. The approach is a refinement of that used in previous studies of itinerant ferromagnetism.[6,29–34] We use a variational wave function $\psi = e^{-J} D$ that is a product of a Slater determinant D, which takes full account of the fermion statistics and includes further electron-electron correlations through a Jastrow factor J. The QMC simulations comprise two stages: First in variational Monte Carlo (VMC) the ground-state energy was minimized by varying the parameters in the Jastrow factor; secondly diffusion Monte Carlo (DMC) starts from the VMC wave function, and treats the Schrödinger equation as a diffusion equation to project out the exact ground state subject to a fixed node approximation.

The Slater determinant $D = \det(\{\psi_{\mathbf{k} \in k_{F\uparrow}}, \bar{\psi}_{\mathbf{k} \in k_{F\downarrow}}\})$ consists of plane-wave orbitals $\psi_{\mathbf{k}}(\mathbf{r}) = \exp(i\mathbf{k} \cdot \mathbf{r})$ whose momenta $\mathbf{k}$ satisfy periodic boundary conditions in the square simulation cell, and lie within the up/down spin Fermi surfaces $k_{F\sigma}$. With a square simulation cell, to ensure that within VMC we have a real-valued wave function and that the Fermi surface is circular, the number of states must correspond to closed shells containing $N_\sigma = \{1,5,9,13,21,25,29,37,45,49\}$ electrons, thus constraining us to discrete values of the magnetization. For computational efficiency we factorize the Slater determinant into up- and down-spin components,[35] so $D = \det(\{\psi_{\mathbf{k} \in k_{F\uparrow}}\}) \det(\{\bar{\psi}_{\mathbf{k} \in k_{F\downarrow}}\})$. Provided that the orbitals of the minority spin state are the lowest energy orbitals of those in the majority spin state,[36] this is the state with total spin $s = s_z = (N_\uparrow - N_\downarrow)/2$.

The Jastrow factor, $J(\{\mathbf{r}_i\})$, accounts for electron-electron correlations. It has the general form,

$$J(\{\mathbf{r}_i\}) = \sum_{i=1}^{N-1} \sum_{j=i+1}^{N} u(r_{ij}) + p(\mathbf{r}_{ij}), \qquad (2)$$

where the summation over indices $\{i, j\}$ cover all $N = N_\uparrow + N_\downarrow$ electrons, the electron separation is $\mathbf{r}_{ij} = \mathbf{r}_i - \mathbf{r}_j$, and $r_{ij} = |\mathbf{r}_{ij}|$. The Jastrow factor includes the polynomial expansion in electron-electron separation proposed in Ref. [37]:

$$u(r_{ij}) = (L - r_{ij})^3 \Theta(L - r_{ij})$$
$$\times \left[\alpha_0 + r_{ij}\left(\frac{3\alpha_0}{L} - \frac{\Gamma_{ij}}{L^3}\right) + \sum_{l=2}^{N_u} \alpha_l r_{ij}^l \right], \qquad (3)$$

chosen so that it satisfies the Kato cusp conditions at $r_{ij} = 0$, is zero beyond the cutoff length L imposed by the Heaviside function Θ, $\Gamma_{ij} = 1/4$ for equal spin electrons, and $\Gamma_{ij} = 1/2$ for opposite spins, and contains $N_u = 8$ variational parameters $\{\alpha_l\}$. The cutoff length L was chosen to be the largest circle that could be inscribed in the simulation cell. The Jastrow factor also includes a plane-wave expansion,

$$p(\mathbf{r}_{ij}) = \sum_{A=1}^{N_p} a_A \sum_{\mathbf{G}_A^+} \cos(\mathbf{G}_A \cdot \mathbf{r}_{ij}), \qquad (4)$$

where the $\{\mathbf{G}_A\}$ are the reciprocal lattice vectors of the simulation cell belonging to the Ath shell of vectors under the full symmetry group of the Bravais lattice, and the superscript "+" means that if $+\mathbf{G}_A$ is included in the sum then $-\mathbf{G}_A$ is excluded. The summation over A covers $N_p = 8$ shells, with corresponding variational parameters $\{a_A\}$. To broaden the freedom of the variational wave function we also include backflow corrections.[38] These substitute the electron coordinates $\mathbf{r}_i$ in the Slater determinant a new set of collective coordinates $\mathbf{x}_i = \mathbf{r}_i + \boldsymbol{\xi}_i(\{\mathbf{r}_j\})$ where the backflow displacement of electron i is $\boldsymbol{\xi}_i$ given by

$$\boldsymbol{\xi}_i = \sum_{j \neq i}^{N} \mathbf{r}_{ij}\left(1 - \frac{r_{ij}}{L}\right)^3 \Theta(L - r_{ij}) \sum_{k=0}^{N_\eta} c_k r_{ij}^k, \qquad (5)$$

where L is the cutoff length, $N_\eta = 7$ the expansion order, and $\{c_k\}$ the variational parameters. The inclusion of the backflow corrections allows the nodal surface of the wave function to shift and therefore relax the fixed node approximation. To seek the ground state the variational parameters of the trial wave function were numerically optimized within VMC by minimizing the total VMC energy.[39] The optimized VMC wave function was used as the trial state for the DMC calculation.

The DMC method[35] simulates a population of walkers whose evolution is driven by the imaginary time Schrödinger equation to project out the ground-state component of the VMC wave function. The walk is taken in a series of discrete time steps, with walkers branching or annihilating according to the local energy. The choice of time step, the control of the walker population, and the system size can each introduce errors into the final prediction of the ground-state energy. We therefore now address how to minimize each source of uncertainty in turn.

Time step. One can propagate forwards in time exactly by using Green's function Monte Carlo[40–47] but unfortunately the method is computationally expensive.[28,35] Therefore here we employ an approximate Green's function that would become exact in the limit of short time steps τ for the walker evolution. However, the computational effort required to achieve a given uncertainty in the prediction for the ground-state energy increases as $1/\tau$, ruling out the use of infinitesimal time steps in practice. Therefore, where high accuracy is required, we use two different finite time steps $\{\tau_i\}$ and extrapolate to $\tau = 0$ to obtain the ground-state energy. Tests revealed that the time-step error had entered the linear regime at $\tau < 0.01$ (at a Wigner-Seitz radius $r_s = 1$). Here to minimize the uncertainty in the extrapolate we followed the prescription of Lee[48] and ran simulations with time steps $\tau = 0.01$ and $\tau/4 = 0.0025$ for relative durations of 1:8, respectively, and then finally extrapolated to $\tau = 0$.

Population control. To ensure that the population control bias is negligible in all runs the target population exceeded 2000.[49] The number of equilibration steps discarded during the equilibration phase of each DMC calculation was set so that the root-mean-square distance diffused by a typical electron exceeded the simulation cell size.

System size. The VMC and DMC simulations must be performed in a finite-sized simulation cell that is periodically repeated to create an effectively infinite system. However, using the finite-sized simulation cell introduces errors into the final prediction for the energy. The error in the estimated energy due to the finite-sized simulation cell can be divided into three components: single particle kinetic energy, Hartree energy, and exchange-correlation energy. The error in the kinetic energy arises because of the approximation of the circular Fermi surface by the discrete set of k vectors of the closed shells within the simulation cell. As the system is enlarged the k-vector grid becomes more fine resulting in abrupt changes in the kinetic energy. The use of a nonzero simulation cell Bloch wave vector $\mathbf{k}_s$ that causes some k vectors to lie outside of the Fermi surface, and others within can lead to a dramatic reduction in the finite-size error, with the optimal being the Balderreschi point.[50] However, it is even better to take an average expectation over all Bloch vectors $\mathbf{k}_s$ within the first Brillouin zone.[49] We adopted the most optimal strategy which is to average over a uniform grid of twists (we use 1000 points) centered on the Balderreschi point of the simulation cell Brillouin zone.[49] The Hartree energy is negligible due to the short-ranged nature of the interaction whose maximum exponential decay length is 1/20 of the typical simulation cell size. The final contribution to the finite-sized error is due to long-range two-body corrections. The change in kinetic energy can be encapsulated by the Chiesa-Holzmann-Martin-Ceperley approximation.[51] It has been shown that in two dimensions the scaling with long-ranged interactions is $\sim N^{-5/4}$ whereas the with short-ranged interaction such as our screened Coulomb interaction the scaling is expected to be $\sim N^{-2}$.[34,49] We also note that it has been found that other expectation values such as magnetic susceptibility can suffer more from finite-size effects, but here we focus only on the ground-state energy.[52]

To gauge the scale of the finite-size error we ran tests on a paramagnetic system with the screened Coulomb interaction
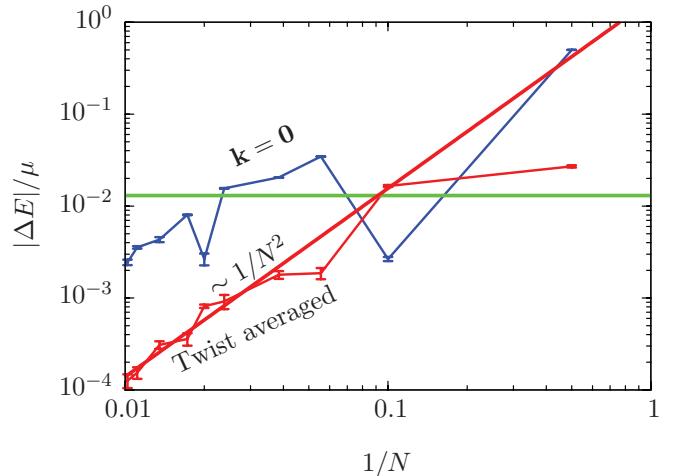

FIG. 2. (Color online) The error in energy ΔE for the $\mathbf{k} = \mathbf{0}$ (blue) and twist averaged (red) calculations with system size (N) for the screened Coulomb potential with $b = 0$, $g/g_{MF} = 0.5$. The red dotted line shows the $\sim 1/N^2$ scaling. The green dashed line shows the energy resolution required to determine the order of the ferromagnetic transition.

with $b = 0$ and $g/g_{MF} = 0.5$ and vary the system size by changing the number of electrons N. Figure 2 shows that twist averaging delivers an error in the energy (determined against a $1/N^2$ extrapolation to the infinite-sized system at $1/N = 0$) that is over an order of magnitude smaller than that from taking just the single result calculated at $\mathbf{k} = \mathbf{0}$. The scaling $1/N^2$ appears similar to that found in a previous two-dimensional study with short-ranged interactions.[34] For the typical system size used $2/N < 0.02$ the finite-sized error is almost two orders of magnitudes smaller than the smallest energy scale $\Delta E \approx 0.012$ that we will need to resolve the features of the phase transition [see Figs. 3(a) and 3(b)]. For large magnetization the energy associated with the minority spin species will have a finite-size correction that scales as $1/N^2_{minority}$ but since that species now makes only a small contribution to the overall energy it is beyond the order needed. Therefore twist averaging ensures that finite-sized errors are inconsequential when analyzing the phase diagram. Finally we note that all of our twist-averaged energies are always slight over estimates of the true energy since the single-particle kinetic energy $k^2/2$ is a convex function and the occupied k space is a convex polyhedron.[49]

Changing polarization. Previous studies of ^{3}He have established that Slater-Jastrow wave functions overestimate the unpolarized state energy, thus favoring the ferromagnetic state. Including many-body backflow corrections can help reduce the energy of the unpolarized state to better align with experiment.[53,54] Here we include two-atom backflow corrections, that for short-ranged interactions have previously been found to have a relatively small impact in the ground-state energy versus that for long-ranged interactions,[34,55] indicating that the QMC bias towards unpolarized states is less for shorter-ranged interactions. However, we also note that an alternative calculation on a lattice with a smaller fixed node bias indicates that the ferromagnetic transition is infinite order rather than first order.[56]
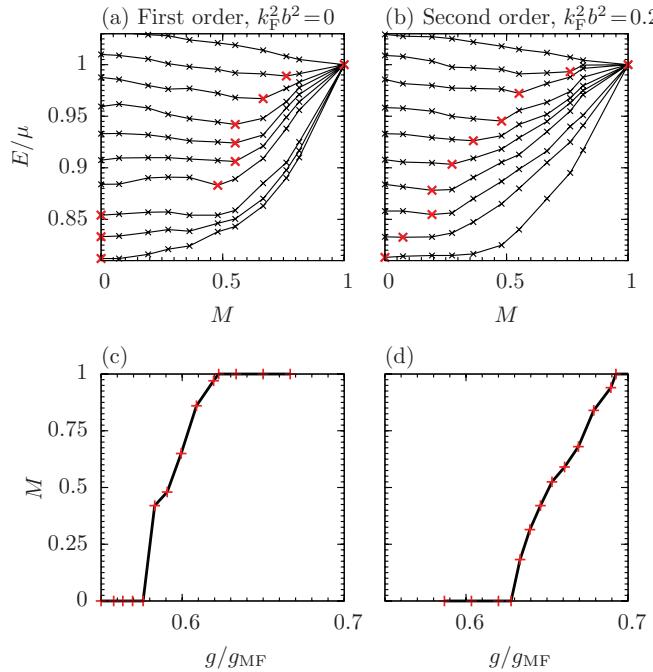
FIG. 3. (Color online) (a) and (b) Energy bands as a function of magnetization M at the interaction strengths shown in (c) and (d) for the screened Coulomb potential (the lowest band is the weakest interaction strength). The red points highlight the minimum point in each energy band. The error bars are approximately the line width. (c) and (d) Magnetization as a function of interaction strength across the transition. The left-hand plots are at $k_F^2 b^2 = 0$, and the right-hand plots at $k_F^2 b^2 = 0.2$.

B. Analytical formalism

The itinerant ferromagnet has previously been analyzed using a functional integral formalism. This will provide a useful complementary tool to study the ferromagnetic transition. The formalism calculates the quantum partition function from a coherent state field integral,

$$
\mathcal{Z} = \int \mathcal{D}\psi \exp\Big[-\sum_{p,\sigma=\{\uparrow,\downarrow\}} \overline{\psi}_{p,\sigma}(-\mathrm{i}\omega + \xi_{\mathbf{p}\sigma})\psi_{p,\sigma}
$$
$$
-\sum_{p_\uparrow,p_\downarrow,q} g(\mathbf{p}_\uparrow - \mathbf{p}_\downarrow)\overline{\psi}_{p_\uparrow-q/2,\uparrow}
$$
$$
\times \overline{\psi}_{p_\downarrow+q/2,\downarrow}\psi_{p_\downarrow-q/2,\downarrow}\psi_{p_\uparrow+q/2,\uparrow} \Big], \qquad (6)
$$

where the field ψ describes a two-component Fermi gas. We now decouple the quartic interaction term with a Hubbard-Stratonovich transformation into the full vector magnetization $\boldsymbol{\phi}$ and the density channel ρ.[7] This is the simplest decoupling scheme that maintains rotational spin invariance and yields the correct Hartree-Fock equations.[57,58] With the action now quadratic in the Fermionic degrees of freedom we integrate them out to recover the quantum partition function $\mathcal{Z} = \int \mathcal{D}\boldsymbol{\phi}\mathcal{D}\rho \exp(-S)$ with the action given by

$$
S = \mathrm{Tr}[\boldsymbol{\phi}\hat{g}\boldsymbol{\phi} - \rho\hat{g}\rho]
$$
$$
- \mathrm{Tr}\ln[(\hat{\partial}_\tau + \hat{p}^2/2 - \mu + \hat{g}\rho)\mathbf{I} - \hat{g}\boldsymbol{\phi}\cdot\boldsymbol{\sigma}].
$$

Here we have employed the operator form of the interparticle potential $\hat{g}$. We adopt $\mathbf{M}$ and ρ_0 as the putative saddle point values of the fields $\boldsymbol{\phi}$ and ρ, and then expand to quadratic order in the fluctuations in those fields about the assumed saddle point. This allows us to integrate out the fluctuations in the magnetization and density channels while keeping terms up to second order in the interaction strength.[6,7,59] This yields the free energy,[7]

$$
F = \sum_{\mathbf{p},\sigma} \frac{p^2}{2} n_{\mathbf{p}\sigma} + \sum_{\mathbf{p}_\uparrow,\mathbf{p}_\downarrow} g(0) n_{\mathbf{p}_\uparrow\uparrow} n_{\mathbf{p}_\downarrow\downarrow}
$$
$$
+ \sum_{\mathbf{p}_1+\mathbf{p}_2=\mathbf{p}_3+\mathbf{p}_4} g^2(\mathbf{p}_1-\mathbf{p}_3) \frac{n_{\mathbf{p}_1\uparrow} n_{\mathbf{p}_2\downarrow}(n_{\mathbf{p}_3\uparrow}+n_{\mathbf{p}_4\downarrow})}{\xi_{\mathbf{p}_1\uparrow}+\xi_{\mathbf{p}_2\downarrow}-\xi_{\mathbf{p}_3\uparrow}-\xi_{\mathbf{p}_4\downarrow}},
$$
$$
(7)
$$

where the first term corresponds to the kinetic energy [with a Fermi distribution $n_{\mathbf{p}\sigma} = 1/(1 + \mathrm{e}^{\xi_{\mathbf{p}\sigma}/T})$, $\xi_{\mathbf{p}\sigma} = p^2/2 - \mu - \sigma g M$, and T is the temperature], the second is the mean-field contribution of the interactions, and the third higher order interaction effects. The first two terms would be delivered by the standard Stoner mean-field theory, and the final term is attributed to fluctuation corrections.[7] We have opted, without loss of generality, to set the quantization axis along the direction of the magnetization. This expression for the free energy remains a function of the magnetization and density, that can now be determined by minimizing the free energy with respect to M and ρ, thereby fulfilling our premise that these are the saddle point values. Since the Fermi distributions have a temperature dependence we can use the formalism to not only study $T = 0$, but also the phase behavior at finite temperature. The formalism applies not only at zero temperature, but also at finite temperature, thus allowing us to map out the entire phase diagram.

The screened Coulomb interaction in momentum space is $g(p) = g/\sqrt{1 + b^2 p^2}$. We have included the effect of finite ranged interactions into the free energy following the prescription in Ref. 59, where it was applied to a three-dimensional system. The mean-field term interaction strength is independent of momentum exchange so is left unaffected by the screening length b. In the fluctuation correction term the denominator means that dominant contributions to the momentum summation arise at $|\mathbf{p}_1 - \mathbf{p}_3| = \sqrt{2}k_F$[6,59] so that we can simply adopt this fixed value within the interaction $g(\mathbf{p}_1 - \mathbf{p}_3) \mapsto g(\sqrt{2}k_F)$, and therefore in the presence of screening the fluctuation correction term is simply rescaled by a factor of $1/(1 + 2k_F^2 b^2)^2$.[6,59] Here we use the definition $k_F = \sqrt[3]{3\pi^2(n_\uparrow + n_\downarrow)}$ where n_σ is the density of the electrons with spin σ. Following this rescaling, the ground-state magnetization can again be extracted by minimizing the free energy with respect to magnetization.

III. RESULTS

With both the quantum Monte Carlo and analytical formalism in place we are well positioned to study the emergent phase diagram. We first focus on the screened Coulomb potential relevant for the solid state, before looking at the cold atom gas.

A. Solid state

We first study the screened Coulomb interaction relevant for the solid state. With a short-ranged interaction $k_F b \ll 1$, the Fourier transform is momentum independent so we recover the contact interaction limit. We performed DMC calculations to determine the ground-state energy for several different values of magnetization and interaction strength, plotting the energy bands in Fig. 3(a). The minimum in each band reveals the magnetization at that interaction strength. With rising interaction strength the magnetization jumps from zero to $M \approx 0.45$, characteristic of a first-order transition. This gives the magnetization with interaction strength curve in Fig. 3(c) that demonstrates not only the first-order transition, but how the magnetization subsequently grows into the fully polarized state. The prediction of a magnetic transition at $g/g_{MF} = 0.57$ is in good agreement with the Eq. (7) prediction of a first-order transition at $g/g_{MF} = 0.51$, that was also found in a previous analytical study.[1]

We next repeat the procedure with a larger screening length $k_F^2 b^2 = 0.2$. Figures 3(b) and 3(d) shows that the magnetization grows smoothly with interaction strength, demonstrating a second-order transition within the magnetization resolution of our QMC calculations. We summarize our results for several screening lengths in the phase diagram in Fig. 4(a). This demonstrates how upon increasing the screening range the critical interaction strength increases and the transition reverts from first to second order. This trend is in good agreement with the analytical predictions from Eq. (7), though the analytical formalism predicts that the transition remains first order due to the presence of a logarithmic divergence in the free energy $F \sim |M|^3 \log(T)$.[1,3–5]

In order to probe the question of the order of the transition more closely, in Fig. 4(b) we show the magnetization formed at the first-order transition as a function of the screening length $k_F^2 b^2$, predicted by both QMC and from the analytical formalism. The analytical formalism predicts a magnetization that falls rapidly with screening length because of the screening reducing the fluctuation correction term that was responsible for driving the first-order transition at a lower interaction strength, but the transition remains first order due to the logarithmic divergence in the free energy. The magnetization following a first-order transition with the contact interaction is predicted to be smaller by QMC, and drops to zero at $k_F^2 b^2 = 0.2$, at which point the transition becomes second order. However, since the QMC method is able to sample the magnetization only at discrete values, $M \in \{0, 0.07, 0.19, 0.28, \ldots\}$, the minimum magnetization that can be formed in a first-order transition is $M_{min} = 0.19$. Due to the rapid decay in the magnetization formed following the first-order transition with screening length, we cannot resolve whether QMC predicts a first- or second-order transition at $k_F^2 b^2 > 0.1$, however, the predicted crossing of the boundary $M_{min} = 0.19$ predicted at $k_F^2 b^2 \approx 0.1$ by QMC and $k_F^2 b^2 \approx 0.18$ from analytics is consistent.

The DMC results have good qualitative agreement with our analytical formalism at $T = 0$. This gives us confidence to use the analytics to study the phase behavior at finite temperature. Figures 1 and 4(c) show that the interaction strength of the transition increases with temperature as the

(a) Zero temperature phase behavior
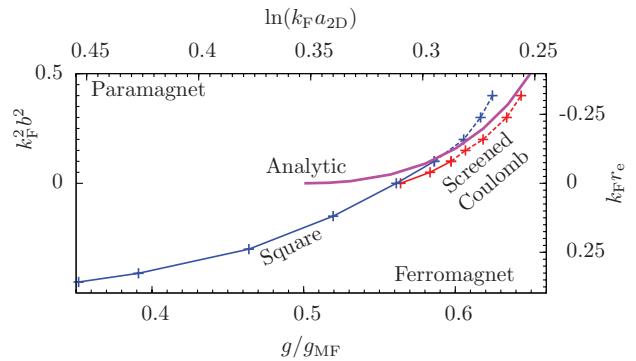
(b) Zero temperature first order transition
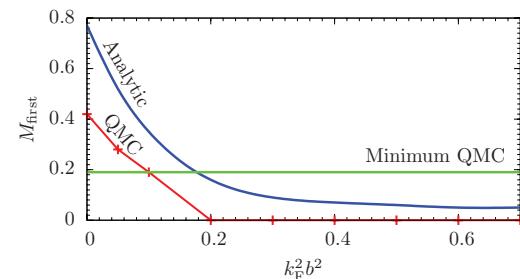
(c) Finite temperature phase behavior
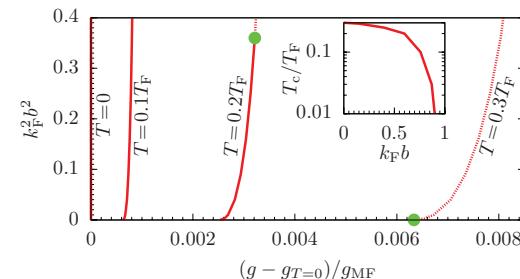
FIG. 4. (Color online) (a) Zero temperature phase behavior. Phase boundary for the emergence of ferromagnetism with varying interaction strength (g/g_{MF}, primary x axis) and screening length ($k_F^2 b^2$, primary y axis) at zero temperature. The secondary x axis and y axis show the parameters relevant for cold atom gases. The solid line corresponds to a first-order transition, and the dashed line a second-order transition. The red line shows the boundary for the screened Coulomb interaction, and the blue line for the square potential. The magenta solid line shows the analytical result for the first-order transition with a screened Coulomb interaction. (b) Zero temperature first-order transition. The magnetization at the first-order transition as a function of Coulomb screening length calculated with QMC (red) and analytically (blue). The green line shows the minimum magnetization of a first-order transition that can be resolved within QMC. (c) Finite temperature phase behavior. The shift in the phase boundary interaction strength, $g - g_{T=0}$ from the screened Coulomb interaction zero temperature analytical phase boundary shown in [(a), magenta solid line] at finite temperatures $T \in \{0, 0.1, 0.2, 0.3\}T_F$ calculated using the analytical formalism. The red solid lines denote a first-order transition and the dotted red line a second-order transition, and the green dots the tricritical points. The inset shows the tricritical point temperature with screening length.

fluctuation correction term is depressed.[1] The trend remains the same with increasing screening length. However, with increasing temperature the transition reverts from first to second order, and the inset of Fig. 4(c) reveals that the tricritical point temperature reduces markedly with increased screening length.

B. Cold atom gas

We now study the possible emergence of ferromagnetic correlations in an ultracold atomic gas. The electrons are simulated by a two-component gas of fermionic atoms, that are mapped onto pseudo-up- and down-spin species. The interactions between the atoms are controlled using a Feshbach resonance. This gives experimentalists access to not only a range of different interaction strengths but also the effective range of the interparticle potential,[17] that can be either positive or negative depending on both the elements and the Feshbach resonance used. In a cold atom gas the parameter used to characterize the interaction strength is the two-dimensional scattering length a_{2D} that can be related to the interaction strength used within the Coulomb interaction by $\ln(k_F a_{2D}) = g_{MF}/2\pi g$, and the effective range is linked to the Coulomb interaction screening length by $r_e = -b^2/a$. However, this gives us access to only negative effective ranges $r_e \leqslant 0$. To study a positive effective range we turn to the square potential $U\theta(R-r)$ to model the interactions. Not only will this allow us to study positive effective range, it will also serve as a useful point of comparison to the results for the screened Coulomb interaction. The square potential has a two-dimensional scattering length a_{2D} given by $\ln(k_F a_{2D}) = (g_{MF}/8\pi^2 R)/[1 - \tanh(\chi)/\chi]$ with $\chi = R\sqrt{U}$, and effective range,

$$r_e = \frac{R}{6}\left(9 + \left[1 - \frac{\tanh\chi}{\chi}\right]^{-2}\right.$$
$$\left. - 3\left[\frac{1}{\chi} + 4\right]\left[1 - \frac{\tanh\chi}{\chi}\right]^{-1}\right). \quad (8)$$

We now use DMC calculations to determine the ground state in the presence of the square well potential. This allows us to augment the phase diagram in Fig. 4. The critical interaction strength and the emergence of the second-order transition are similar for both the square well potential and our previous study of the screened Coulomb interaction, though the square potential can be extended to effectively negative $k_F^2 b^2$. This verifies the form of our phase diagram, and confirms that irrespective of the interparticle potential our main result of the transition changing from first to second order with rising screening length within the resolution of our simulations,

accompanied by a rise in the critical interaction strength is robust.

The persistence of the ferromagnetic transition from negative into positive effective ranges $k_F r_e$ makes the two-dimensional gas a tantalizing target in the search for ferromagnetism in a cold atom gas. Recent experiments have shown that atomic gases with a large negative effective range[17] have greatly suppressed two- and three-body losses. Our predictions of the changing magnetization in Figs. 3 and 4(b) could be measured through phase contrast imaging that would reveal the growing polarization in the emerging domains.[21] Our accurate determination of the phase boundary through DMC calculations, complemented by analytical predictions, should guide future experiments.

IV. DISCUSSION

In this paper we have outlined quantum Monte Carlo calculations on the two-dimensional itinerant ferromagnet. The calculations show that the system undergoes a paramagnet to ferromagnet phase transition. The transition is first order for interactions with a short effective range, and within our magnetization resolution second order for interactions characterized by longer effective ranges. We have reconciled this with the damping effect that long-range interactions have on the quantum fluctuations. We have compared the DMC results to an analytical formalism and found good agreement, allowing us to then use the analytic formalism to extend the phase diagram to finite temperatures. Higher temperatures suppress the first-order behavior leading to a tricritical point at $T = 0.3T_F$, whose temperature reduces with increasing screening length.

With typical solid-state experimental systems having a screening length $0.5 \leqslant k_F b \leqslant 1$,[10,60] the first-order transition should still be visible but with the fluctuation correction term tempered, and thus the associated tricritical temperature will be reduced. This could reduce the tricritical point seen in theory $0.3T_F$ to the $0.02T_F$ seen in experiments on both two- and three-dimensional materials[8–15] and increase the visibility of exotic low temperature phases that are promoted by quantum criticality such as the spin spiral and p-wave superconductor.

[1]G. J. Conduit, Phys. Rev. A **82**, 043604 (2010).

[2]J. Hertz, Phys. Rev. B **14**, 1165 (1976).

[3]D. V. Efremov, J. J. Betouras, and A. Chubukov, Phys. Rev. B **77**, 220401(R) (2008).

[4]D. Belitz, T. Kirkpatrick, and T. Vojta, Rev. Mod. Phys. **77**, 579 (2005).

[5]D. L. Maslov, A. V. Chubukov, and R. Saha, Phys. Rev. B **74**, 220402(R) (2006).

[6]G. J. Conduit, A. G. Green, and B. D. Simons, Phys. Rev. Lett. **103**, 207201 (2009).

[7]G. J. Conduit and B. D. Simons, Phys. Rev. A **79**, 053606 (2009).

[8]S. Ikeda, Y. Maeno, and T. Fujita, Phys. Rev. B **57**, 978 (1998).

[9]R. S. Perry, K. Kitagawa, S. A. Grigera, R. A. Borzi, A. P. Mackenzie, K. Ishida, and Y. Maeno, Phys. Rev. Lett. **92**, 166602 (2004).

[10]I. I. Mazin and D. J. Singh, Phys. Rev. Lett. **79**, 733 (1997).

[11] N. Kikugawa, C. Bergemann, A. P. Mackenzie, and Y. Maeno, Phys. Rev. B **70**, 134520 (2004).

[12] F. Nakamura, T. Goko, M. Ito, T. Fujita, S. Nakatsuji, H. Fukazawa, Y. Maeno, P. Alireza, D. Forsythe, and S. R. Julian, Phys. Rev. B **65**, 220402(R) (2002).

[13] A. Huxley, I. Sheikin, E. Ressouche, N. Kernavanois, D. Braithwaite, R. Calemczuk, and J. Flouquet, Phys. Rev. B **63**, 144519 (2001).

[14] S. Watanabe and K. Miyake, J. Phys. Chem. Solids **63**, 1465 (2002).

[15] S. S. Saxena, P. Agarwal, K. Ahilan, F. M. Grosche, R. K. W. Haselwimmer, M. J. Steiner, E. Pugh, I. R. Walker, S. R. Julian, P. Monthoux, G. G. Lonzarich, A. Huxley, I. Sheikin, D. Braithwaite, and J. Flouquet, Nature (London) **406**, 587 (2000).

[16] G.-B. Jo *et al.*, Science **325**, 1521 (2009).

[17] C. Kohstall, M. Zaccanti, M. Jag, A. Trenkwalder, P. Massignan, G. M. Bruun, F. Schreck, and R. Grimm, Nature (London) **485**, 615 (2012).

[18] A. Schirotzek, C.-H. Wu, A. Sommer, and M. W. Zwierlein, Phys. Rev. Lett. **102**, 230402 (2009).

[19] R. A. Duine and A. H. MacDonald, Phys. Rev. Lett. **95**, 230403 (2005).

[20] L. J. LeBlanc, J. H. Thywissen, A. A. Burkov, and A. Paramekanti, Phys. Rev. A **80**, 013607 (2009).

[21] G. J. Conduit and B. D. Simons, Phys. Rev. Lett. **103**, 200403 (2009).

[22] D. Pekker, M. Babadi, R. Sensarma, N. Zinner, L. Pollet, M. W. Zwierlein, and E. Demler, Phys. Rev. Lett. **106**, 050402 (2011).

[23] C. Sanner, E. J. Su, W. Huang, A. Keshet, J. Gillen, and W. Ketterle, Phys. Rev. Lett. **108**, 240404 (2012).

[24] C. W. von Keyserlingk and G. J. Conduit, Phys. Rev. A **83**, 053625 (2011).

[25] G. J. Conduit and E. Altman, Phys. Rev. A **82**, 043603 (2010).

[26] S. K. Baur and N. R. Cooper, Phys. Rev. Lett. **109**, 265301 (2012).

[27] V. K. Thankappan, *Quantum Mechanics* (New Age International, New Delhi, 1993).

[28] R. J. Needs, M. D. Towler, N. D. Drummond, and P. López Ríos, J. Phys.: Condens. Matter **22**, 023201 (2010).

[29] D. M. Ceperley and B. J. Alder, Phys. Rev. Lett. **45**, 566 (1980).

[30] G. Ortiz, M. Harris, and P. Ballone, Phys. Rev. Lett. **82**, 5317 (1999).

[31] F. H. Zong, C. Lin, and D. M. Ceperley, Phys. Rev. E **66**, 036703 (2002).

[32] S. Pilati, G. Bertaina, S. Giorgini, and M. Troyer, Phys. Rev. Lett. **105**, 030405 (2010).

[33] S.-Y. Chang, M. Randeria, and N. Trivedi, Proc. Natl. Acad. Sci. USA **108**, 51 (2011).

[34] N. D. Drummond, N. R. Cooper, R. J. Needs, and G. V. Shlyapnikov, Phys. Rev. B **83**, 195429 (2011).

[35] R. Needs, M. Towler, N. Drummond, and P. López Ríos, computer program CASINO, Version 2.3 User Manual (University of Cambridge, Cambridge, 2008); W. M. C. Foulkes, L. Mitas, R. J. Needs, and G. Rajagopal, Rev. Mod. Phys. **73**, 33 (2001).

[36] C. C. J. Roothaan, Rev. Mod. Phys. **32**, 179 (1960).

[37] N. D. Drummond, M. D. Towler, and R. J. Needs, Phys. Rev. B **70**, 235119 (2004).

[38] P. López Ríos, A. Ma, N. D. Drummond, M. D. Towler, and R. J. Needs, Phys. Rev. E **74**, 066701 (2006).

[39] C. J. Umrigar, J. Toulouse, C. Filippi, S. Sorella, and R. G. Hennig, Phys. Rev. Lett. **98**, 110201 (2007).

[40] M. H. Kalos, Phys. Rev. **128**, 1791 (1962).

[41] M. H. Kalos, J. Comput. Phys. **1**, 257 (1966).

[42] M. H. Kalos, D. Levesque, and L. Verlet, Phys. Rev. A **9**, 2178 (1974).

[43] D. M. Ceperley, M. H. Kalos, and J. L. Lebowitz, Macromolecules **14**, 1472 (1981).

[44] P. J. Reynolds, D. M. Ceperley, B. J. Alder, and W. A. Lester, J. Chem. Phys. **77**, 5593 (1982).

[45] D. M. Ceperley and B. J. Alder, J. Chem. Phys. **81**, 5833 (1984).

[46] D. M. Ceperley and M. H. Kalos, *Monte Carlo Methods in Statistical Physics*, 2nd ed., edited by K. Binder (Springer, Berlin, 1986).

[47] K. E. Schmidt and M. H. Kalos, *Applications of Monte Carlo Methods in Statistical Physics*, 2nd ed., edited by K. Binder (Springer, Berlin, 1987).

[48] R. M. Lee, G. J. Conduit, N. Nemec, P. López Ríos, and N. D. Drummond, Phys. Rev. E **83**, 066706 (2011).

[49] N. D. Drummond, R. J. Needs, A. Sorouri, and W. M. C. Foulkes, Phys. Rev. B **78**, 125106 (2008).

[50] A. Baldereschi, Phys. Rev. B **7**, 5212 (1973).

[51] S. Chiesa, D. M. Ceperley, R. M. Martin, and M. Holzmann, Phys. Rev. Lett. **97**, 076404 (2006).

[52] M. Holzmann, B. Bernu, V. Olevano, R. M. Martin, and D. M. Ceperley, Phys. Rev. B **79**, 041308(R) (2009).

[53] F. H. Zong, D. M. Ceperley, S. Moroni, and S. Fantoni, Mol. Phys. **101**, 1705 (2003).

[54] M. Holzmann, B. Bernu, and D. M. Ceperley, Phys. Rev. B **74**, 104510 (2006).

[55] N. D. Drummond and R. J. Needs, Phys. Rev. B **79**, 085414 (2009).

[56] G. Carleo, S. Moroni, F. Becca, and S. Baroni, Phys. Rev. B **83**, 060411(R) (2011).

[57] J. Hubbard, Phys. Rev. B **19**, 2626 (1979).

[58] R. E. Prange and V. Korenman, Phys. Rev. B **19**, 4691 (1979).

[59] C. W. von Keyserlingk and G. J. Conduit, arXiv:1301.6036.

[60] G. Santi, S. B. Dugdale, and T. Jarlborg, Phys. Rev. Lett. **87**, 247004 (2001).